

I. Da Riva and A. Sanz

Condensation in Ducts

Phase changing flows are being considered for thermal management in space platforms. The resulting flow patterns are very complicated and extremely sensitive to gravity action.

Concerning fluid flow in ducts, the available evidence indicates that although the pressure loss does not depend too much on the fluid flow pattern, the heat transfer (and resulting phase change) does.

A simple exercise to illustrate this point is presented in this paper. It deals with condensing flow in straight circular cross-sectional ducts.

Two extreme configurations are considered here, one corresponds to a stratified flow and the other to an annular flow. Both types of flow patterns have been extensively considered in the past and from this point of view almost nothing is new in the paper, but past results look conflictive and this could be due to the limitations and computational intricacies of the models used. Thus the problem has been reformulated from the onset and the results are presented as the evolution of the vapor quality (vapor to total mass flow rate) along the duct, in typical cases.

The results presented here indicate that within the validity of the present models and the assumed ranges of mass flow rate, duct diameter, thermal conditions and fluid characteristics, the length of the ducts required to achieve complete condensation under zero gravity are an order of magnitude larger than in horizontal tubes under normal terrestrial conditions.

1 Introduction

The flow in ducts out of evaporators would be dominated by condensation. Normal gravity enhances condensation because body forces help drive the condensed liquid. Thence, condensation in ducts under reduced gravity is much less efficient than that inside horizontal ducts under normal gravity.

The flow patterns in either case differ substantially, fig. 1. Regarding this figure, it should be said that the stratified (fig. 1a) and the annular (fig. 1b) flow patterns are the most common ones under normal and under reduced gravity conditions respectively and are taken here as typical. Other flow patterns exist depending on the flow conditions. The definition of these flow patterns and of their boundaries have been much debated. The reader should be addressed to basic texts on the field such as [1] or [2], among others.

Mail address: Prof. A. Sanz, Laboratorio de Aerodinámica, E.T.S.I. Aeronáuticos, Univ. Politécnica, Pza. Cardenal Cisneros, s/n, E-28040 Madrid, Spain.

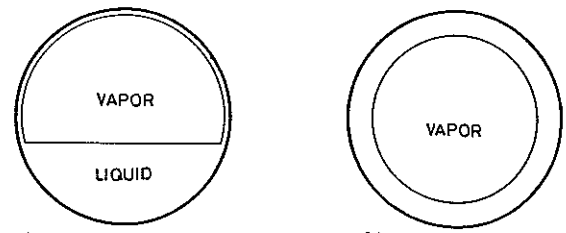

Fig. 1. Flow geometry when gravity is (a) dominant, in a horizontal tube, and (b) negligible. The void fraction (vapor fractional area in the figure) is the same in both cases

A comparison of condensing flows inside ducts under normal and under reduced gravity conditions has been already attempted [3]. The basic difference between the two cases results from the stratified condensate layer which appears in horizontal ducts when gravity is dominant (fig. 1a) and which is almost inactive in the heat transfer process, whereas the thin condensate film formed in the duct is very effective. When gravity effects are negligible (fig. 1b) the annular flow pattern prevails and the much thicker layer is less effective than the thin condensate which appeared in fig. 1a.

The present paper is organized as follows. The relevance of two-phase flow for the thermal management systems of large space platforms is briefly introduced in sec. 2. This will focus the present study on space applications.

Then a fairly general model of condensing nearly one-dimensional fluid flow is introduced in sec. 3. Particular attention is paid to the wall friction and heat transfer phenomena.

The mentioned general model is particularized to the stratified flow case in sec. 4. To this aim the work of *Ruffer* and *Kezios* [4] is followed except that gas friction at the wall (which is dominant at the high vapor quality end of the tube) and gas momentum are taken into account. The addition of these terms allows to avoid a singularity at the starting of condensation which appears in the model of *Ruffer* and *Kezios*.

The annular flow case is then worked out by use of well known heat transfer models [5] and [6] in sec. 5. A comparison between the results furnished by either model is presented as a support in the selection of the seemingly more appropriate model.

The evolution of the vapor quality, w, along the duct is then calculated in either case for five typical fluids and under thermal conditions close to those chosen in [3], but with much higher flow rates (as in [4]) closer to the values relevant to the large space platforms requirements.

The results presented in this paper seem to indicate that the condensation enhancing effects of gravity are, at the flow rates considered, much larger than those presented in [3].

2 Two-phase Flow in Large Space Platforms

The thermal management systems of future space platforms will require the transfer of kilowatts of thermal energy at distances of over 50 m to remote radiators, with small temperature differences. Many of the systems proposed to cope with these requirements employ a two-phase fluid loop to transport the thermal energy.

Using the latent heat of fluids, orders of magnitude more heat can be transferred, under nearly isothermal conditions, than is possible using the sensible heat of single phase fluids.

In recent years many possible candidate options have been considered in the literature [7, 8]. The trade-offs performed included different working fluids (either single or two-phase), interfaces with the heat loads, pumping systems, thermal storage, and radiators for heat rejection. In these studies the degree of promise of the different options is measured against comprehensive criteria.

A comparison between single and two-phase ammonia loops for a high power space platform is presented in [8]. The fluid inventory, required flow rates, pumping power and pipe diameters are considerably reduced for two-phase systems, which on the other hand are intrinsically isothermal. However, when the radiator is included the two-phase systems show no significant advantages since the radiator mass is the dominant term.

Although many investigations have been done to determine the criteria for the design of a two-phase flow system, one of the unknown areas is the behaviour of two-phase flows in a reduced gravity environment. The nature of the flow, the geometry of the flow system and the properties of the fluids all have significant influence. Then the designer is

List of Symbols

A_{FL} internal cross-sectional area of a duct [m^2]
A_G gas filled part of the cross-sectional area of a duct [m^2]
A_L liquid filled part of the cross-sectional area of a duct [m^2]
D diameter [m]
Fr Froude number $Fr = \dfrac{m^2}{\varrho_L^2 A_{FL}^2 Dg}$
Nu liquid Nusselt number $Nu = \dfrac{h_m D}{k_L}$
N_{TD} *Taitel* and *Dukler* dimensionless group, eq. (10)
Pr liquid Prandtl number $Pr = \dfrac{c_{pL}\mu_L}{k_L}$
Re Reynolds number $Re = \dfrac{4m}{\pi D \mu_G}$
Sf Stefan number $Sf = \dfrac{h_{fg}}{c_{pL}(T_{sat} - T_w)}$
T temperature [K]
T_{sat} liquid-vapor temperature [K]
T_w wall temperature [K]
T^+ dimensionless temperature [K] $T^+ = \dfrac{\varrho_L u^* c_{pL}}{h_m}$
V mean fluid velocity [m s^{-1}]
c_p constant-pressure fluid specific heat [J kg^{-1} K^{-1}]
f Fanning friction factor
g acceleration due to gravity [m s^{-2}]
h_m average convective heat transfer coefficient [W m^{-2} K^{-1}]
h_{fg} heat of vaporization or condensation [J kg^{-1}]
h'_{fg} heat of condensation corrected by partial subcooling effect [J kg^{-1}] eq. (3)
k thermal conductivity [W m^{-1} K^{-1}]
m fluid mass flow rate [kg s^{-1}]
p pressure [Pa]
p_{sat} liquid-vapor pressure [Pa]
q heat flux [W m^{-2}]
u^* friction velocity [m s^{-1}] $u^* = \sqrt{\dfrac{\tau_w}{\varrho}}$
u^+ dimensionless velocity $u^+ = \dfrac{u}{u^*}$
w vapor quality $w = \dfrac{m_G}{m}$
x axial distance to duct entry [m]
z vertical distance above arbitrary datum plane [m]
Π wetted perimeter of a duct [m]
Φ Lockhart-Martinelli pressure loss multiplier
α void fraction $\alpha = \dfrac{A_G}{A_{FL}}$
δ annular film thickness [m]
δ^+ dimensionless film thickness $\delta^+ = \dfrac{\delta u^*}{v}$
μ fluid dynamic viscosity [Pa s]
v fluid kinematic viscosity [m^2 s^{-1}]
ϱ fluid density [kg m^{-3}]
τ_w average shear stress at the wall [kg m^{-1} s^{-2}]
ϕ polar angle of stratified flow interface [°]

Subscripts

F liquid film
G gas
L liquid
SG gas flowing alone in the duct
SL liquid flowing alone in the duct
TP two phase

forced either to operate in flow regimes where gravity is not important, which results in obvious limitations, or to place the liquid in position at 1 g as it would be under reduced g conditions, in order to validate the ground-based test data.

It has been determined from analysis and tests [9] that the trade-off between pipe size and pressure drop favors the transport of the liquid at mass flow rates per unit are near the boundaries of the stratified flow which would exist in a horizontal pipe under normal g conditions.

It should be interesting to compare the condensing stratified flows near the onset of interface instability (where transition to other configurations will appear) to the condensing annular flows, a situation which would prevail under reduced g, for the same fluid, flow rate and temperature level, in straight circular cross-sectional ducts.

Two accounts of already performed (and planned for the near future) experiments on two-phase flow under reduced gravity conditions, in the United States, are given in [10, 11].

3 Condensing Flow Model

In this paragraph a simple unified model of condensing flow inside a duct is introduced. Later on this model will be particularized to the two extreme cases which have been sketched in fig. 1.

The main simplifying assumptions of the model are:

(1) The duct is horizontal.
(2) The *static* pressure is uniform in each cross section.
(3) The liquid flow is assumed to be uniform in each cross section accounting for the effect of film thickening.
(4) The vapor flow is also uniform in each cross section.

Regarding the particularization to the stratified flow case two additional features of the model should be mentioned.

(5) Liquid film thickening implies an axial component of hydrostatic pressure. This effect is accounted for in a way which resembles that in open channel hydraulics although here the vapor pressure could change along the duct [4].
(6) The condensate formed in the film flows down the duct wall and joins the bulk liquid flowing along the bottom of the duct. The liquid film is so thin that it can be neglected both regarding gas flow area and liquid wall friction.

An additional simplifying assumption must be introduced in connection with the fluid thermodynamic and transport properties.

(7) The wall temperature, T_w, is kept constant. On the other hand, the pressure loss is very small compared to the saturation pressure level. Then the fluid saturation pressure and temperature are assumed to be constant along the duct for calculating fluid thermodynamic and transport properties.

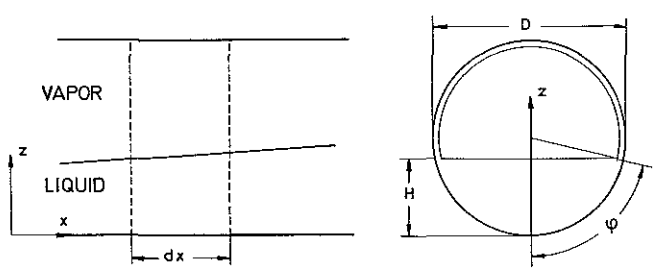

Fig. 2. Geometry used in the model of stratified flow condensation

Fig. 2 summarizes the flow geometry. Although the figure is particularized to the stratified flow case, it is sufficiently general for the present purposes.

The conservation equations in the control volume, which encloses liquid, L, and vapor, G, are:

Mass preservation equation

$$\frac{\mathrm{d}}{\mathrm{d}x}(m_L + m_G) = 0.$$

m_L and m_G are the liquid and vapor mass flow rates, respectively.

Momentum balance equation

$$\frac{\mathrm{d}}{\mathrm{d}x}\left(\varrho_L A_L V_L^2 + \rho_G A_G V_G^2\right) = -\frac{\mathrm{d}p}{\mathrm{d}x} A_{FL} - \varrho_L g \frac{\mathrm{d}}{\mathrm{d}x} \int_{A_L} (H - z) \frac{\mathrm{d}A_L}{\mathrm{d}z}\,\mathrm{d}z - \Pi_L \tau_{wL} - \Pi_G \tau_{wG}. \tag{1}$$

ϱ, A and V indicate density, effective cross-sectional area and (average) velocity of the corresponding fluid phase, respectively. The left hand sides give the change in momentum. The first term on the right hand side is the resultant of the static pressure on the fluid (liquid or vapor) per unit axial length of the control volume. A_{FL} is the internal cross-sectional area of the duct. The second term is the resultant of hydrostatic pressures acting on planes x and $x + \mathrm{d}x$ which enclose different liquid areas. This term disappears in the reduced gravity (annular flow) case. The last two terms are the wall friction of the liquid and vapor, respectively, per unit axial length, here τ_{wL} and τ_{wG} are average shear stresses at the wall, and Π_L and Π_G are the corresponding wetted perimeters.

No force due to phase change at the interface is considered. Condensation is assumed to take place in the peripheral liquid film.

Thermal energy equation

$$h_m(T_{sat} - T_w)A = -h'_{fg} \frac{\mathrm{d}m_G}{\mathrm{d}x}. \tag{2}$$

This equation merely indicates that the heat transfer to the wall, the area of which is $A = \pi D$ per unit length, equals the enthalpy change form saturated vapor to condensate.

h_m is an average heat transfer coefficient.
T_{sat} is the saturated vapor temperature,
T_w the wall temperature and
h'_{fg} the corrected value of the heat of condensation.

The film temperature is nonuniform and slightly below saturation temperature because of partial subcooling of the liquid, then [4]:

$$h'_{fg} = h_{fg} + 0.68\, c_{pL}(T_{sat} - T_w), \tag{3}$$

where c_{pL} is the liquid specific heat.

3.1 Static Pressure Loss

In addition to the terms giving the friction at the wall, which will be introduced in sec. 3.2, eq. (1) exhibits a term which cannot be easily evaluated a priori. This term is the static pressure gradient.

The static pressure gradient is related in [4] to a friction factor via a mixture approximation correlation. Different approximations of the two phase flow based on the single phase flow of a liquid of average properties running full in the duct of diameter D have been suggested in [12]. In any case the pressure loss is related to the friction factor by [13]:

$$\frac{dp}{dx} = -\frac{32m^2 f_{TP}}{\varrho_{TP}\pi^2 D^5}, \tag{4}$$

where f_{TP} is a function of the mixture Reynolds number (of the Poiseuille, Blasius or other type) and the subscript TP indicates two phase. The average single phase flow is considered as laminar when Re_{TP} is less than 2,400 and turbulent otherwise (as it occurs in the single phase flow). The mixture Reynolds number, Re_{TP}, is defined as:

$$Re_{TP} = \frac{4m}{\pi D \mu_{TP}} = \frac{\mu_G}{\mu_{TP}} Re,$$

where Re is the Reynolds number in terms of the gas viscosity. ϱ_{TP}, μ_{TP} are defined as:

$$\varrho_{TP} = (1-\alpha)\varrho_L + \alpha\varrho_G,$$

$$\mu_{TP} = (1-\alpha)\mu_L + \alpha\mu_G,$$

α being the cross-sectional void fraction.

The equations for the calculations of ϱ_{TP} and μ_{TP} are those of special case I in [12]. They correspond to the no-slip restriction $V_L/V_G = 1$. The validity of this restriction is very difficult to appraise but it gives the correct behavior in the two extreme cases, namely, liquid only ($\alpha = 0$) and vapor only ($\alpha = 1$).

Note that, in general, Re_{TP} as well as f_{TP} will depend on α.

3.2 Friction Terms

In order to evaluate the friction terms in the right hand side of eq. (1) we will introduce the usual friction factors at the wall for the liquid and vapor.

$$\tau_{wL} = \frac{1}{2}\varrho_L V_L^2 f_L; \quad \tau_{wG} = \frac{1}{2}\varrho_G V_G^2 f_G,$$

where f_L and f_G will depend on Re_L and Re_G respectively.

The average liquid and gas velocities are:

$$V_L = \frac{m_L}{\varrho_L A_L} = \frac{1-w}{1-\alpha}\frac{m}{\varrho_L A_{FL}};$$

$$V_G = \frac{m_G}{\varrho_G A_G} = \frac{w}{\alpha}\frac{m}{\varrho_G A_{FL}}, \tag{5}$$

w being the vapor quality.

The Reynolds numbers based on the respective hydraulic diameters, $D_{EL} = 4A_L/\Pi_L$ and $D_{EG} = 4A_G/\Pi_G$, can be written as:

$$Re_L = (1-w)\frac{\mu_G}{\mu_L}\frac{\Pi}{\Pi_L} Re; \quad Re_G = w\frac{\Pi}{\Pi_L} Re.$$

Finally, the expressions of the wall friction per unit duct length are, respectively:

$$\Pi_L \tau_{wL} = \Pi_L \frac{1}{2}\left(\frac{1-w}{1-\alpha}\right)^2 \frac{m^2 f_L}{\varrho_L A_{FL}},$$

$$\Pi_G \tau_{wG} = \Pi_G \frac{1}{2}\left(\frac{w}{\alpha}\right)^2 \frac{m^2 f_G}{\varrho_G A_{FL}}. \tag{6}$$

Now the Reynolds numbers, Re_i ($i = L, G$), and then the friction factors, f_i, will depend both on the geometry of the cross sectional liquid-vapor configuration, through Π_L/Π or Π_G/Π, on the vapor quality, w, and on the void fraction, α. It is convenient to express f_L and f_G as:

$$f_L\left(\frac{\Pi_L}{\Pi}, w\right) = f_L\left(\frac{\Pi_L}{\Pi}, 0\right)(1-w)^{L_L};$$

$$f_G\left(\frac{\Pi_G}{\Pi}, w\right) = f_G\left(\frac{\Pi_G}{\Pi}, 1\right) w^{L_G} \tag{7}$$

where $L_i = -1$ when the corresponding flow is laminar or $L_i = -0.25$ when it is turbulent (according to Poiseuille or Blasius formulae) [13].

3.3 Dimensionless Momentum Equation

Bringing eqs. (4)–(7) to eq. (1) we reach:

$$D\frac{d}{dx}\left[\frac{(1-w)^2}{1-\alpha} + \frac{\varrho_L}{\varrho_G}\frac{w^2}{\alpha} + \frac{1}{Fr\, A_{FL} D}\int_{A_L}(H-z)\frac{dA_L}{dz}\,dz\right]$$

$$= 2\frac{\varrho_L}{\varrho_{TP}} f_{TP} - 2\frac{\Pi_L}{\Pi}\frac{(1-w)^{2+L_L}}{(1-\alpha)^2} f_L\left(\frac{\Pi_L}{\Pi}, 0\right)$$

$$- 2\frac{\varrho_L}{\varrho_G}\frac{\Pi_G}{\Pi}\frac{w^{2+L_G}}{\alpha^2} f_G\left(\frac{\Pi_G}{\Pi}, 1\right) \tag{8}$$

where Fr is a Froude number defined as:

$$Fr = \frac{m^2}{\varrho_L^2 A_{FL}^2 D g}.$$

Several terms of eq. (8), which depend on the particular model under consideration, are specified in table 1.

3.4 Dimensionless Energy Equation

Eq. (2) in dimensionless form becomes:

$$D\frac{dw}{dx} = -\frac{4Nu}{Pr\, Re\, Sf}\frac{\mu_L}{\mu_G}, \tag{9}$$

where Nu is the liquid Nusselt number:

$$Nu = \frac{h_m D}{k_L},$$

Pr the liquid Prandtl number:

$$Pr = \frac{c_{pL}\mu_L}{k_L},$$

Re is the, already introduced, Reynolds number based on the gas viscosity, and Sf the Stefan number:

Table 1. Geometry and flow-dependent terms in eqs. (10), (11), and (12)

type of flow	stratified	annular
configuration	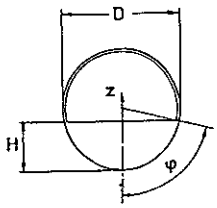	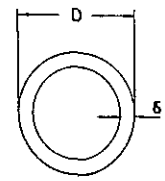
α	$\frac{\pi-\varphi}{\pi}+\frac{\sin 2\varphi}{2\pi}$	$\left(1-\frac{2\delta}{D}\right)^2$
Π_I/Π	$\frac{\varphi}{\pi}$	1
Π_G/Π	$1-\frac{\varphi}{\pi}$	0
$f_L\left(\frac{\Pi_L}{\Pi},0\right)$	$16\frac{\mu_L}{\mu_G}\frac{1}{Re}\frac{\varphi}{\pi}$	$16\frac{\mu_L}{\mu_G}\frac{1}{Re}$
	$0.079\left(\frac{\mu_L}{\mu_G}\frac{1}{Re}\frac{\varphi}{\pi}\right)^{0.25}$	$0.079\left(\frac{\mu_L}{\mu_G}\frac{1}{Re}\right)^{0.25}$
$f_L\left(\frac{\Pi_G}{\Pi},1\right)$	$16\frac{1}{Re}\left(1-\frac{\varphi}{\pi}\right)$	0
	$0.079\left[\frac{1}{Re}\left(1-\frac{\varphi}{\pi}\right)\right]^{0.25}$	0
L_L	-1	-1
	-0.25	-0.25
L_G	-1	–
	-0.25	–
$\frac{1}{Fr\,A_{FL}D}\int_{A_L}(H-z)\frac{dA_L}{dz}\,dz$	$\frac{1}{2\pi\,Fr}\left[\frac{2}{3}\sin^3\varphi-\cos\varphi\left(\varphi-\frac{\sin 2\varphi}{2}\right)\right]$	0
$\frac{4Nu}{Pr\,Re\,Sf}\frac{\mu_L}{\mu_G}$	$\frac{4}{\pi}\left[\frac{2}{3Fr}\left(1-\frac{\varrho_G}{\varrho_L}\right)\left(\frac{\mu_L}{\mu_G}\right)^2\frac{1}{Pr^3Re^2Sf^3}\right]^{1/4}\left[\frac{4}{3}\int_0^{\pi-\varphi}\sin^{1/3}\omega\,d\omega\right]^{3/4}$	$(1-w)\frac{4Nu}{Pr\,Re_L\,Sf}$
comments on Nu	h_m has been expressed by means of a modification of *Nusselt's* result for the outside of horizontal tubes [4], [15]	$Nu=\frac{Nu_{SL}}{1-\alpha}$ $Nu_{SL}=Pr\,Re_L\frac{1}{T^+(\delta^+)}\sqrt{\frac{f_L}{2}}$, eq. (14)

$$Sf = \frac{h'_{fg}}{c_{pL}(T_{sat} - T_w)}.$$

Among these four dimensionless groups, *Nu*, *Pr*, *Re*, *Sf*, only the Nusselt number, *Nu*, depends on the geometry and on the model used (See table 1).

4 Stratified Condensing Flow Model

The particularization of the above equations to the stratified condensing flow model is quite straightforward. The mathematical expressions given in the relevant column of table 1 should be taken into account.

4.1 Variation of the Vapor Quality along the Duct in the Stratified Condensing Flow Model

The autonomous system of differential eqs. (8, 9) with initial conditions

$x = 0, \quad w = 1, \quad \alpha = 1,$

has been numerically integrated in typical cases using a Newton-Raphson scheme. Numerical values for the computations are given in tables 2 and 3 and the results are summarized in figs. 3 and 4.

Table 2. Condensation in ducts. Typical fluid properties; assumed values: $T_{sat} = 300\,K$, $T_{sat} - T_w = 10\,K$

fluid[1]	$(\varrho_G/\varrho_L) \cdot 10^3$	μ_L/μ_G	*Pr*	*Sf*
Freon 11	4.42	37.6	4.21	21.0
Freon 12	29.9	16.5	3.05	14.7
Freon 22	39.6	14.5	2.87	15.0
water	0.0258	94.3	5.86	57.2
ammonia	13.8	12.3	1.42	24.7

[1] Data for *Freon* 11, 12, and 22 as well as for ammonia are from [16]. Those for water are from [17].

The model is no longer valid in the neighborhood of $w = 0$ where, according to the results presented in fig. 3, the void fraction, α, does not vanish. Arriving at this final situation would imply large pressure variations which will

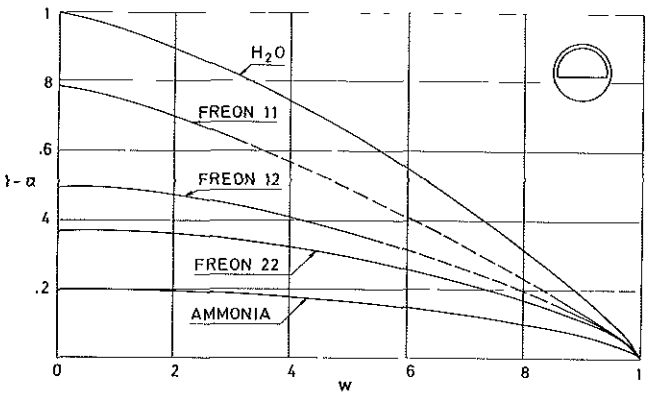

Fig. 3. Liquid fraction, $1 - \alpha$ vs. vapor quality, w, for stratified condensing flow of several liquids along horizontal ducts. Solid line: stratified smooth regime; dashed line: stratified-wavy regime

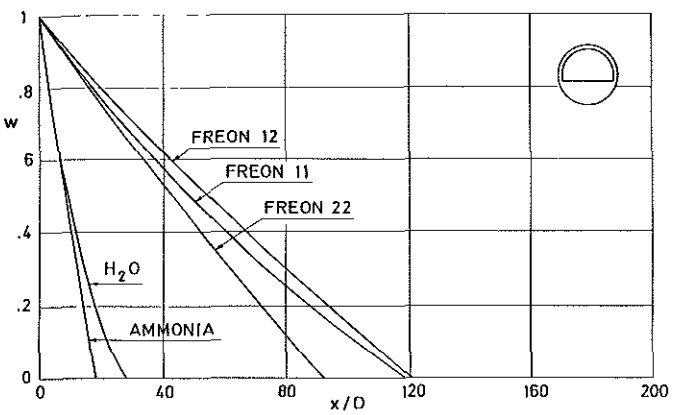

Fig. 4. Vapor quality, w, vs. dimensionless distance along the duct, x/D, for stratified condensing flow of several liquids along horizontal ducts

Table 3. Condensation in ducts. Parameters depending on m and D; assumed values $mh_{fg} = 10^3\,W$, $D = 16.1 \cdot 10^{-3}\,m$; stratified case

fluid	$m \cdot 10^3$ [kg s^{-1}]	$Fr \cdot 10^3$	$Re \cdot 10^{-3}$	$\left(\frac{4Nu}{a(\varphi)Pr\,Re\,Sf}\frac{\mu_L}{\mu_G} \cdot 10^3\right)^2$	N_{TD}^3
Freon 11	5.54	2.17	39.8	5.67	0.766
Freon 12	7.26	4.74	44.2	4.84	0.914
Freon 22	5 55	3.36	32 5	5.95	2.02
water	0.410	0.0259	3 56	33.5	10.6
ammonia	0.864	0.317	5.97	27.0	35 4

[2] $a(\varphi) = \left[\frac{4}{3}\int_0^{\pi-\varphi} \sin^{1/3}\omega\, d\omega\right]^{3/4}, \quad a(0) = 2.53$

[3] see eq. (10).

conflict with simplifying assumption 7 in sec. 3. The effect is purely local and has not been investigated further.

4.2 Limits of Validity of the Stratified Model

The stratified condensing flow model, which has been introduced, is based on the assumption of the stability of the liquid-vapor interface. This means that the points of coordinates m_G/A_{FL}, m_L/A_{FL} representing any cross-section in the flow-regime map must be enclosed in the domain corresponding to that particular flow pattern [1, 2].

Among the flow maps which are available those in [14] are very convenient for the present purposes since the transitions between different regimes are given by means of analytical expressions.

The transition between the so-called stratified-smooth and stratified-wavy regimes appears when the vapor velocity is sufficiently large to produce small surface waves.

The criterion given in [14] for the onset of instability reads, in our variables,

$$\frac{w^2(1-w)}{\alpha^2(1-\alpha)} > N_{TD}\,, \tag{10}$$

where

$$N_{TD} = 400\,\frac{\varrho_G}{\varrho_L}\left(1-\frac{\varrho_G}{\varrho_L}\right)\frac{\mu_L}{\mu_G}\,\frac{1}{Re\,Fr}$$

is a dimensionless group already tabulated in table 3.

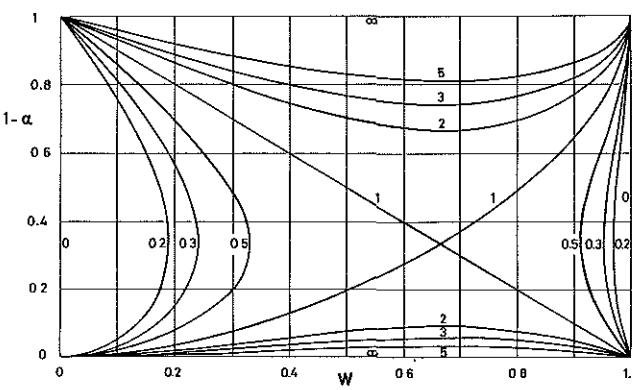

Fig. 5. The Taitel and Dukler limit for stratified smooth flow in the $1-\alpha$ vs. w plane. Figures on the curves represent constant values of the parameter $w^2(1-w)/\alpha^2(1-\alpha)$ which appears in eq. (10)

Curves of constant values of the ratio $w^2(1-w)/\alpha^2(1-\alpha)$ in the $(1-\alpha)$ vs. w plane have been represented in fig. 5. In order to assess the validity of the stratified-smooth flow model we superimpose figs. 3 and 5 taking into account (10) and the values of N_{TD} given in table 3. The change of regime can be shown in fig. 3.

5 Annular Condensing Flow Model

In the case of the annular flow, the mathematical formulation is quite parallel to that in the previous paragraphs. Now the geometrical parameter is the film thickness, δ.

The mass preservation equation remains the same as in sec. 3.

The momentum balance equation can be deduced from eq. (8) with $1/Fr = \Pi_G = 0$. The gaseous friction terms have not been retained because in annular condensation there are no contacts between gas and walls.

$$D\,\frac{\mathrm{d}}{\mathrm{d}x}\left[\frac{(1-w)^2}{1-\alpha}+\frac{\varrho_L}{\varrho_G}\,\frac{w^2}{\alpha}\right]$$
$$= 2\,\frac{\varrho_L}{\varrho_{TP}}\,f_{TP} - 2\,\frac{\Pi_L}{\Pi}\,\frac{(1-w)^{2+L_L}}{(1-\alpha)^2}\,f_L\left(\frac{\Pi_L}{\Pi}\,,0\right) \tag{11}$$

The thermal energy equation is again eq. (10) although the heat transfer mechanism is different here.

The average heat transfer coefficient h_m can be expressed as [15]:

$$h_m = h_{SL}\,\Phi_L\,,$$

where h_{SL} is the heat transfer coefficient which would exist if the liquid were flowing alone through the tube with the same flow rate,
Φ_L is the Lockhart-Martinelli pressure loss multiplier. In the annular flow case [18]:

$$\Phi_L = \frac{1}{1-\alpha}\,.$$

Eq. (9) is still valid as thermal energy equation in dimensionless form, although in the annular flow case

$$Nu = \frac{Nu_{SL}}{1-\alpha}\,,$$

where Nu_{SL} is the Nusselt number if the liquid mass flow rate were flowing alone through the tube.

This simple expression behaves correctly at both ends of the process. When $\delta/D \ll 1$ the definition of the liquid Nusselt number in terms of the hydraulic diameter of the liquid annulus would be:

$$Nu_{SL} = \frac{h_m 4\delta}{k_L}\,,$$

then

$$Nu = \frac{Nu_{SL}}{\dfrac{4\delta}{D}}\,,$$

which agrees with the previous expression of Nu when $\delta/D \ll 1$.

The agreement at the other end is obvious; when $\alpha \to 0$, $Nu \to Nu_{SL}$.

5.1 Heat Transfer Coefficient in Annular Flow

Different correlations are available for calculating the heat transfer coefficient h_m inside horizontal or slightly inclined tubes in the annular flow regime. It would be interesting to compare two of the most often used before selecting that appropriate for our purpose.

(1) duct average heat transfer coefficient, h_m:

Boyko and *Kruzhilin* [5] on the basis of their extensive data with $1.2 \cdot 10^6$ Pa to $9 \cdot 10^6$ Pa steam over a liquid Reynolds number range of $6 \cdot 10^3$ to $3 \cdot 10^5$ suggest the following correlation for the average Nusselt number, $\overline{Nu}$

$$\overline{Nu} = \frac{0.024}{(1-w)^{0.8}} Pr^{0.43} Re^{0.8} \left(\frac{1+\sqrt{\varrho_L/\varrho_G}}{2}\right). \quad (12)$$

This correlation is also recommended for other than steam-water systems in the same (liquid) Prandtl number range (0.9 to 3).

(2) correlation for h_{SL}:

These correlations have been used widely in liquid flow heat transfer calculations.

Kosky and *Staub* [6] give the local Nusselt number in the liquid-alone case in terms of the friction velocity $u^* = \sqrt{\tau_w/\varrho}$, and in terms of the dimensionless temperature function $T^+(\delta^+)$. The friction velocity, u^*, becomes:

$$u^* = \sqrt{\frac{D}{4\varrho_L}\left(-\frac{dp}{dx}\right)},$$

whereas the dimensionless temperature, $T^+(\delta^+)$, is defined as:

$$T^+(\delta^+) = \frac{\varrho_L u^* c_{pL}}{h_m},$$

$\delta^+ = \delta u^*/\nu$ is a dimensionless film thickness.

This correlation is based on the Martinelli analogy between turbulent momentum and heat transfer.

$T^+(\delta^+)$ is given by the following sequence of equations:

$$T^+(\delta^+) \begin{cases} = \delta^+ Pr, & \text{for } \delta^+ \le 5, \\ = 5\left\{Pr + \ln\left[1 + Pr\left(\frac{\delta^+}{5} - 1\right)\right]\right\}, & \text{for } 30 \ge \delta^+ > 5, \\ = 5\left\{Pr + \ln(1 + 5Pr + 0.495 \ln\left(\frac{\delta^+}{30}\right)\right\}, & \text{for } \delta^+ > 30, \end{cases} \quad (13)$$

whereas the dimensionless film thickness, δ^+, is given by

$$\delta^+ \begin{cases} = \sqrt{\frac{Re_L}{2}} & \text{for } Re_L < 1000, \\ = 0.0504 Re_L^{7/8} & \text{for } Re_L > 1000. \end{cases} \quad (13a)$$

The liquid-alone local Nusselt number, $Nu_{SL}(x)$, can be written as

$$Nu_{SL}(x) = Pr\, Re \frac{1}{T^+(\delta^+)} \sqrt{\frac{f_L}{2}}, \quad (14)$$

where the liquid-alone friction factor is

$$f_L \begin{cases} = \frac{16}{Re_L} & \text{for } Re_L < 1000, \\ = 0.079 Re^{-0.25} & \text{for } 1000 < Re_L < 10^5. \end{cases}$$

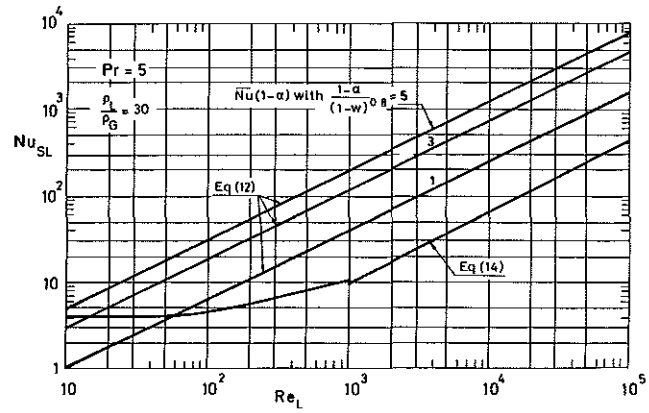

Fig. 6. Liquid-alone Nusselt number, Nu_{SL}, vs. liquid Reynolds number, Re_L, as given by different correlations in typical cases

Different curves of the liquid-alone Nusselt number, Nu_{SL}, given by the above correlations are shown as functions of Re_L for typical values of Pr and ϱ_L/ϱ_G and, when required, of $(1-\alpha)/(1-w)^{0.8}$ in fig. 6.

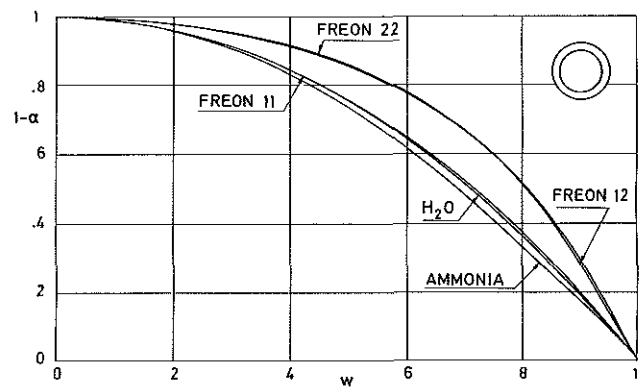

Fig. 7. Liquid fraction, $1-\alpha$, as a function of vapor quality, w, for annular flow of several liquids along ducts

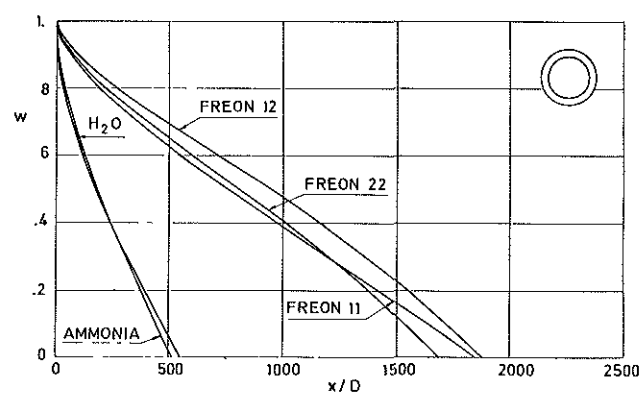

Fig. 8. Vapor quality, w., vs. dimensionless distance along the duct, x/D, for annular flow of several liquids along ducts

4.2 Variation of the Vapor Quality Along The Duct in the Annular Model

The autonomous system of differential eqs. (9) and (11), with the mathematical expressions given in the column labelled *annular* of table 1 and in eqs. (13) and (13a), is numerically integrated as in the stratified flow case (sec. 3.1).

Results are given in figs. 7 and 8.

A difficulty could appear, however, near the origin ($x = 0$: $w = \alpha = 1$), where the liquid is still absent and the vapor contacts the walls of the duct. Since the onset of condensation is not included in the model, the problems associated with the transition of Π_L/Π from 1 to 0 are eluded starting the numerical integration slightly apart from $x = 0$ with $\Pi_G/\Pi = 0$ and $\Pi_L/\Pi = 1$.

A comparison of figs. 4 and 8 clearly indicates the large enhancing effect of gravity on condensation. This effect results to be considerably larger than that previously predicted [3]. It could be due to differences in the model (gas friction and momentum were not considered in [3]) and in the flow regimes (flow regimes in [3] occurs at very low Reynolds numbers).

5. Conclusions

Heat transfer in ducts with phase change is being considered for thermal management in the just coming space platforms. This applications poses several problems mainly related with the poor knowledge of the flow pattern under reduced gravity which will influence the heat transfer process.

A very simple example has been presented here by means of computations based on two well known and widely documented models of the two phase flow in ducts one stratified and the other annular. It is seen that, under the validity of the models used, an order of magnitude increase in dimensionless tube length (x/D) is required to achieve complete condensation in a duct under reduced gravity as compared with a horizontal duct under normal gravity.

Acknowledgements

This paper resulted from the work supported by the European Space Agency in the preparation of the Spacecraft Thermal Control Design Data Handbook, ESA (TST-02), Rev. 4. 1988. ESA Contract (ESTEC/6115/84/NL/MA).

References

1 *Govier, G. W., Aziz, K.:* The Flow of Complex Mixtures in Pipes, Van Nostrand Reinhold Company, New York, 1972.
2 *Hetsroni, G.:* Handbook of Multiphase Systems, Hemisphere Publishing Corporation, Washington, 1982.
3 *Keshock, E. G., Sadeghipour, M. S.;* Acta Astronautica 10, 505 (1983).
4 *Rufer, C. E., Kezios, S. P.:* Heat Transfer 88, 265 (1966).
5 *Boyko, L. D., Kruzhilin, G. N.:* Int. J. Heat Mass Transfer 10, 361 (1967).
6 *Kosky, P. G., Staub, F. W.:* A.I.Ch.E. Journal 17, 1037 (1971).
7 *Van Oost, S., Mathieu, J. P.:* in: ESA Report CR(P) 1873 (1983).
8 *Sadunas, J. A., Lehtinen, A., Parish, R.:* AIAA Paper No. 85-1047 (1985).
9 *Fowle, A. A.:* AIAA Paper No. 81-1075 (1981).
10 *Best, F. R.:* in: Progress in Astronautics and Aeronautics, Vol. 122, American Institute of Aeronautics and Astronautics, Inc., Washington, p. 291–332 (1990).
11 *Krotiuk, W. J., Antoniak, Z. I.:* in: Progress in Astronautics and Aeronautics, Vol. 122, American Institute of Aeronautics and Astronautics, Inc., Washington, p. 173–221 (1990).
12 *Dukler, A. E., Wicks III, M., Cleveland, R. G.;* A.I.Ch.E. Journal 10, 44 (1964).
13 *Schlichting, H.:* Boundary Layer Theory, McGraw-Hill Book Company, Inc., New York, 1960.
14 *Taitel, Y., Dukler, A. E.:* A.I.Ch.E. Journal 22, 47 (1976).
15 *Butterworth, D.:* in: Heat Exchangers. Bergles, A. E., Mayinger, F. (Eds.), Hemisphere Publishing Corporation, Washington, p. 289–313 (1981).
16 ASHRAE; Handbook. 1985. Fundamentals, American Society of Heating, Refrigerating and Air Conditioning Engineers, Inc., Atlanta, GA (1985).
17 *Schmidt, E.:* Properties of Water and Steam in SI-Units, Springer Verlag, Berlin (1969).
18 *Wallis, G. B.:* One-Dimensional Two-Phase Flow. McGraw-Hill Inc., New York, 1969.

J. A. Nicolás

Frequency Response of Axisymmetric Liquid Bridges to an Oscillatory Microgravity Field

The dynamical response of nearly-cylindrical liquid bridges when subjected to an oscillatory microgravity field has been studied. The analysis has been performed by using a linear three-dimensional model, valid for columns of arbitrary slenderness. Theoretical results are presented and compared with previous ones of a one-dimensional slice model showing that the validity of the slice model is restricted to slender columns.

1 Introduction

The liquid bridge problem has been extensively studied either from a theoretical or from an experimental point of view as is reflected in the number of publications on this subject (see [1]).

Some theoretical models have already been developed for studying the free oscillations of liquid columns (see [2]). There are some important differences between the models for infinite columns, based on the jet-stability theory [3–6] and the models for finite columns [2, 7, 8], as pointed out in [2]. The capillary jet models are unable to fulfil the boundary conditions at the disks and the one-dimensional models for finite columns are limited to slender columns.

In this paper we used a linear three-dimensional model in order to study the frequency response of axisymmetric liquid bridges to an oscillatory microgravity field. This model is similar to that previously employed to obtain the free frequencies of axisymmetric liquid columns [2]. Although other analysis of dynamical response of liquid bridges to microgravity disturbances have been published [9, 10], these studies are based on one-dimensional models and, therefore, restricted to slender columns, while the model here presented retains all the significant characteristics of the phenomenon (in the inviscid case), being also appropriate for short columns. Finally, the results obtained have been compared with those of the above-mentioned theoretical models [9, 10], showing quite good agreement for slender columns.

Mail address: J. A. Nicolás, Departamento de Fundamentos Matemáticos, E.T.S.I Aeronáuticos, Universidad Politécnica, E-28040 Madrid, Spain.

2 General Inviscid Equations

We consider a liquid bridge held by surface tension between two parallel, coaxial, equal-diameter solid disks, surrounded by a vacuum of gas with far lower density than the liquid, as shown in fig. 1.

To study the frequency response of nearly-cylindrical liquid bridges to an oscillatory microgravity field, we assume the following: inviscid liquid, uniform and constant liquid density, ϱ, as well as surface tension, σ, and axisymmetric configuration and perturbations.

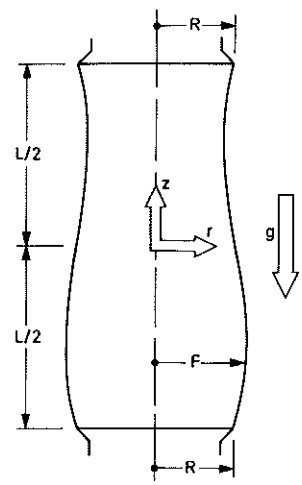

Fig. 1. Geometry and coordinate system for the liquid bridge

In the following, all physical quantities are made dimensionless using the disk radius, R, as characteristic length, and $(\varrho R^3/\sigma)^{1/2}$ as characteristic time. There are two dimensionless parameters: the slenderness of the liquid bridge, $\Lambda = L/2R$, and the Bond number, $B = \varrho g R^2/\sigma$, which measures the microgravitational effects.

Under such assumptions, the flow is irrotational, therefore the velocity field can be considered to be derived from a velocity potential, $\phi(r, z, t)$, that satisfy the Laplace equation:

$$\Delta\phi = 0; \tag{1}$$

and the pressure field is related to the velocity potential through the generalized Bernoulli equation:

$$P = -\phi_t - \tfrac{1}{2}(\nabla\phi)^2 - Bz. \tag{2}$$